Maria Sklodowska-Curie Actions (MSCA)
Innovative Training Networks (ITN)
H2020-MSCA-ITN-2018
Grant number 813137

Project number 813137

URBASIS-EU
New challenges for Urban Engineering Seismology

DELIVERABLE

Work Package: WP2
Number: D2.3 – Development of Physical-Based Ground Motion Model for Induced Seismicity, Case Study: Preston New Road, UK

Authors:	**Suroyo, Pungky**	(UoL)
Co-Authors:	Edwards, Benjamin	(UoL)

Reviewers	Bindi, Dino
Approval	Management Board
Status	Final Version
Dissemination level	Public
Delivery deadline	31.01.2023
Submission date	01.03.2023
Intranet path	https://urbasis-eu.osug.fr/Scientific-Reports-157

URBASIS-EU

Table of Contents

Abstract

The shale gas site at Preston New Road (PNR), near Blackpool, UK, has experienced shallow and small magnitude earthquakes causing some damage, observed mainly through cosmetic damage to structures in the surrounding areas. Quantifying risk assessment is important to reduce the possible threats of further, possibly larger, earthquakes. Better risk quantification will be influenced by a better determination of seismic hazard in the study area. Improvement of seismic hazard assessment through adapting and adjusting the available ground motion prediction equations (GMPEs) for near field- shallow earthquakes has been evaluated in this study, specifically for the PNR site. Stochastic simulation was performed for the development of an application-specific ground motion model for induced earthquakes in the PNR gas field by considering a new physically- based seismic attenuation model obtained from spectral fitting approach. The comparison between the new ground motion model (GMM) in the present study, with existing GMPEs from previous study, and GMPEs developed from other induced seismicity environments is presented. The comparison with the GMPE for tectonic seismicity provides explanation of the difference characteristic of ground motion model for near field- shallow earthquake and the deeper tectonic earthquake.

Introduction

Seismic events can produce injuries and fatalities, damage to buildings or infrastructure, in addition to interruptions to business and operation. To mitigate and reduce the potential threats of earthquakes, it is important to perform risk analysis and develop methodology and/or scenario to better manage earthquakes. The quantification of seismic risk requires quantification of seismic hazard as the input. Hazard assessment was carried out by studying local geology, tectonic settings, past historic earthquakes or seismicity of the area, and magnitude levels. This is necessary to estimate the intensity and ground shaking hazard that may occur in the various parts of the city.

The study and application of hazard estimation has evolved in recent decades through the identification of epistemic uncertainties (related with unknown knowledge) and introduction of a rational frameworks for handling the apparent randomness in earthquake processes (Bommer, 2022). Despite the escalation of the hazard assessment studies, there are still several challenges found. One of the examples is the seismic hazard estimation for low-seismicity regions such as the

United Kingdom (UK). The lack of earthquake strong-motion records in the low-to moderate magnitude seismicity regions, such as the UK, means that trivial methods to estimate a GMPE for strong ground motion is no longer valid (Edwards et al.,2008). The selection of suitable existing GMPE and the adaptation for specific region become more profound in the case of anthropogenic earthquakes. This deliverable aims to improve our understanding of ground motions from induced seismicity in Blackpool, UK, and in particular, about the difference of ground motion characteristics between induced and UK regional seismicity. This comparison will help to better explain the bias observed (Edwards et al., 2021; Douglas et al.,2013) in the adapted regional GMPEs applied in the induced seismicity case.

The first section of this deliverable will cover a brief description about induced seismicity and its impact on seismic hazard analysis, and the state of the art of the ground motion models for induced seismicity applications. The overview of our datasets is explained in the second section. Finally, we review existing GMPEs for induced seismicity and present a new ground motion model, developed using physical-based stochastic simulations, for the PNR region.

Induced Seismicity

Induced seismicity, has become a more commonly discussed and pertinent topic for study in recent years due to a significant increase in the number of anthropogenic earthquakes. Historically, the first observation of induced seismicity was connected to mining activities in South Africa in early 1894 (Müller et al., 2021; McGarr et al, 2002). Davis & Frolich (1993), proposed a series of questions to classify as induced seismic or not. The term 'anthropogenic seismicity’ can be considered where human activity is reasonably shown to be the cause, or at least a major influence, of earthquakes. Such anthropogenic earthquakes can be subdivided into ‘triggered’ and ‘induced’ events. Triggered events are predominantly of natural origin since the state of stress in the area is tending toward the condition of shear failure. In this case, human activity simply accelerates the fault’s inevitable failure. Meanwhile, induced events are generated purely by human activity (Rietbrock et al., 2013).

According to ‘The Human-Induced Earthquake Database’ (HiQuake) there are 1239 projects reported to have generated induced earthquakes, with 33% dominated by fracking activities and 25% (the second highest proportion) due to mining activities. This total number has increased by

58.9% from last documentation by Wilson, et al. (2017), which reported a total ~730 projects associated with induced seismicity. In this case, the highest contributions were mining (37%) and the impoundment of water behind dams (23%). The injection activities and fracking account for ~10-15% of cases in this previous analysis. The fastest-growing anthropogenic activity is clearly induced earthquakes generated by fracking. This study will focus on ground motions that occur most-likely due to hydraulic fracturing. Hydraulic fracturing is commonly performed by drilling into tight-shale formations and injecting fluids under pressure to enable the production of oil and gas from previously unproductive formations (Ellsworth, 2013); The increase in pore pressure on a fault that can result from fluid injection reduces the effective normal stress acting on the fault and lowers the resistance to shearing, which can lead to a fault's rupture.

Impact of Induced Seismicity on Seismic Hazard Analysis

Despite of the small magnitude generated, induced seismicity can generate damage and become a concern. Shallower focal depths than tectonic seismicity, means shorter travel path from source to the surface, thus, generating higher ground motions than a deeper tectonic earthquake. Perceptible ground motion associated with industrial activities can cause distress to those who are affected, especially if there are many repeated episodes of shaking. This small magnitude event can cause public threat, damage to infrastructure, and affect interruption to business and operation and generate financial losses. Regardless of the understanding of the impact and possible risk due to induced seismicity, the implication of induced earthquake in the calculation of seismic hazard analysis remains unclear. One solution proposed by Walters, et al. (2015) is a site-specific and adaptable hazard and risk assessment and traffic-light protocol for injection projects.

The traffic-light system (TLS) is typically used to address the possibility of a variable seismic risk over time and allow for real-time risk management. Either the injection projects are recommended to continue (green), modify or re-evaluate due to increased risk (amber), or suspend operations due to severe risk (red). The fundamental purpose of a TLS is to avoid levels of ground shaking that would exceed tolerable limits, which would generally mean anything from causing damage to buildings in the vicinity of operation to causing a disturbance to the local populations. These site-specific protocols and assessments are useful for operations, but the question remains as to how the increasing rate and magnitudes of induced events will affect future assessments of seismic hazard. Probabilistic seismic hazard assessment (PSHA) for induced seismicity can adapt PSHA studies of natural seismicity, where earthquake rates and ground motions are inferred from past observation or historical earthquakes catalogues. However, for induced seismicity, the equivalent observational metric is not the average numbers of earthquakes per year resulting from continuous long-term tectonic processes, but it is rather related to operational parameters such as pumping volume and pressure and the susceptibility of the subsurface to induced seismicity. The estimation of hazard for future operational scenarios is enhanced by relating the observations of induced earthquakes to a characteristic of the fluid injection, for example by using the seismogenic index (Shapiro et al., 2010), which relates the seismic activity rate to the total volume of injected fluid.

Ground Motion Prediction for Induced Seismicity

For many years, ground motion models (GMM) have been developed for application to tectonic earthquakes of magnitude 4.5 or greater. Extrapolation of such equations, derived from regression of data from larger magnitude earthquakes, has been shown to overestimate ground motions not only for smaller magnitudes, but even at the lower limit of the target magnitude range (Bommer, et al. 2007; Chiou, et al. 2010; Chiou and Youngs 2014; Douglas and Jousset 2011; Baltay and Hanks 2014). For induced seismicity, several GMPEs have been proposed, such as: (1) Dost et al. (2004) who developed GMPE derived from recordings of shallow induced earthquakes in the Netherlands; (2) Sharma et al. (2014) who recognised the need of application-specific GMPEs and derived predictive equation to estimates ground motion for induced seismic in The Geysers geothermal field in California; and (3) Douglas, et al. (2013) who derived empirical and stochastic equations using earthquake recordings resulting from shallow geothermal activity.

In many cases, ground motion models for induced seismicity were adapted from existing tectonic ground motion models. Atkinson & and Assatourians (2017) demonstrate the use of California tectonic earthquakes with depth between 2-6 km to approximate ground motion for induced seismicity in Central and Eastern North America (CENA) by introducing near-distance saturation for small-to-moderate earthquakes, and explicitly consider source parameters as a function of focal depth in the model’s functional form. Atkinson (2015) developed a GMPE using tectonic data, but limited to short distances and shallow depths, for use in induced seismicity settings.

An important question to consider is then the applicability of ground motion models, developed from tectonic earthquake, to estimate motions from induced events. Using a similar GMPE form to Atkinson (2015), Gupta et al. (2017) found that application of this model to induced seismicity in Central and Eastern United states (CEUS) results in a good fit for hypocentral distances up to 60 km. Yenier & and Atkinson (2015) found that for the same tectonic setting and focal depth, ground motion for natural and induced earthquake appears to be similar. On the other hand, McNamara et al. (2019), while evaluating GMMs for USGS seismic hazard forecast: 'Induced and Tectonic earthquakes in the Central and Eastern United States', concluded that Next Generation Attenuation (NGA)-East GMMs and 2014 CEUS GMMs show better performance for CEUS tectonic earthquakes than induced earthquakes. The model proposed by Atkinson (2015) and Grazier (2017) score better for predicting CEUS induced earthquake ground motions (Farajpor, 2021). However, it appears that these models overpredict ground motion in the distance range of 10-40 km. Similar observation were found by Bommer, et al. (2016) for induced seismicity due to gas field compaction in Groningen, where the initial GMPE, borrowed from the neighbouring field, as developed by Dost et al. (2004), did not provide a good fit to the data.

Data and Data Processing

A total of 192 events with 57 events ($-0.8 \leq M_L \leq 1.5$) recorded in 2018 associated with hydraulic fracturing at PNR-1z and 135 events ($-1.7 \leq M_L \leq 2.9$) recorded during the second phase at PNR-2 in 2019 were used for the induced seismic dataset in this study (Figure 1). These records were captured from several sensors from different networks (LV, PNR, SD, and UR) spread within 20 km from the PNR Shale Gas Site (Figure 2). Induced events were located at shallow depths of up to 4 km, with epicentral distances up to 20 km (Figure 3).

An additional dataset (network GB) from natural earthquake records was provided by the British Geology Survey (BGS). We henceforth refer to this as the tectonic dataset (Figure 4). This dataset consists of 308 events with magnitudes $-1.4 \leq M_L \leq 4.2$ recorded in 2019. This dataset also contains small magnitude (M<0) and shallow earthquake identified as tectonic earthquakes which was recorded near Charlwood, England, UK. This location close to the two actively operating oilfield discovery and production sites at Brockham and Horse Hill (Hicks, et al., 2019). These anomalous seismic swarms occurring at shallow depth can have natural causes (e.g., Bent et al., 2017; Hicks et al., 2019). Catalogue of this dataset can be accessed through BGS website (https://www.earthquakes.bgs.ac.uk/), while detailed information can be downloaded from ftp://seiswav.bgs.ac.uk/events in Nordic file format. By joining event information and station information, the complete catalogue was generated. Event waveforms were then retrieved from the daily continuous 'mseed' files provided from the BGS repository. Most of the records presented in this study come from the BGS network, due to the limited access of the data from other networks (Figure 5). These records spread from 0 - 700 km, with focal depths up to 28 km (Figure 6).

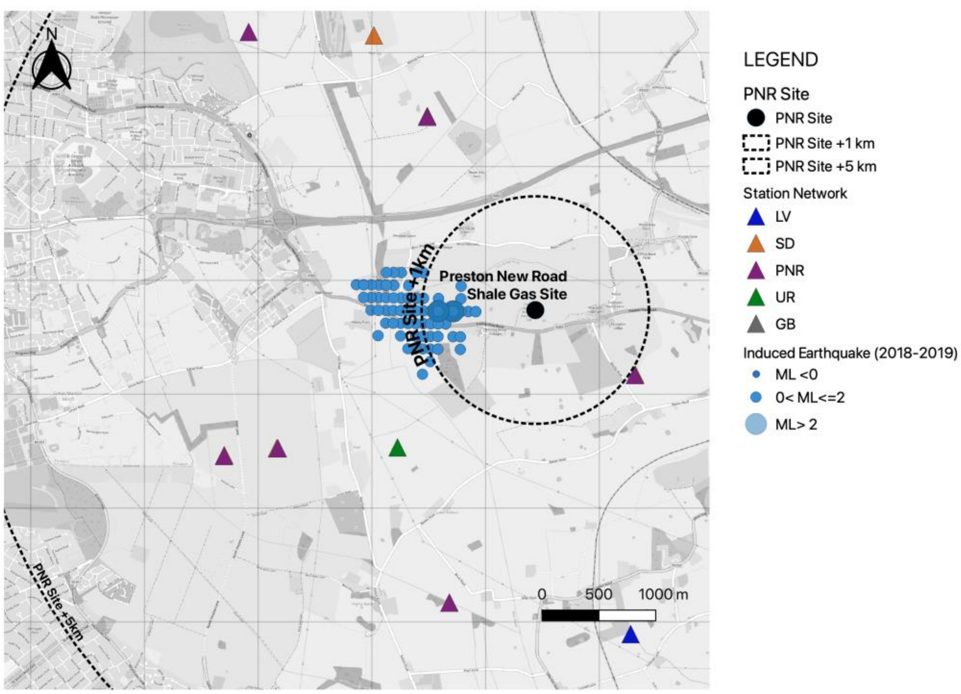

Figure 1. Map of stations and induced event locations (recorded in 2018-2019 from Preston New Road site with local magnitude range $-1.7 \leq M\_L < 3$.

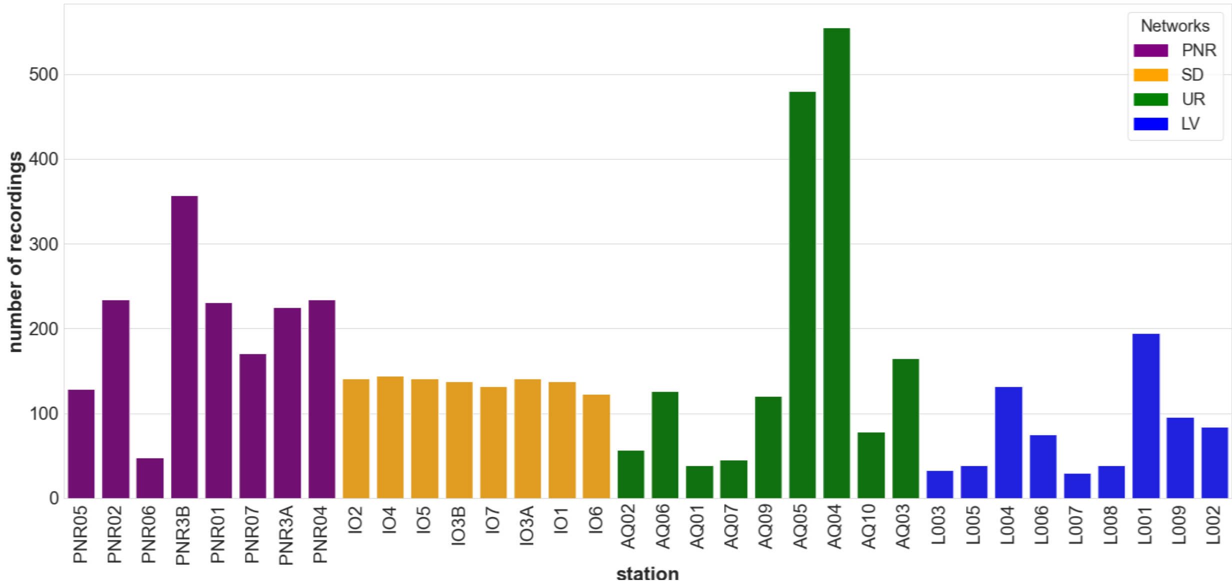

Figure 2. Number of recordings for each different stations for induced dataset. Colours indicate each different network.

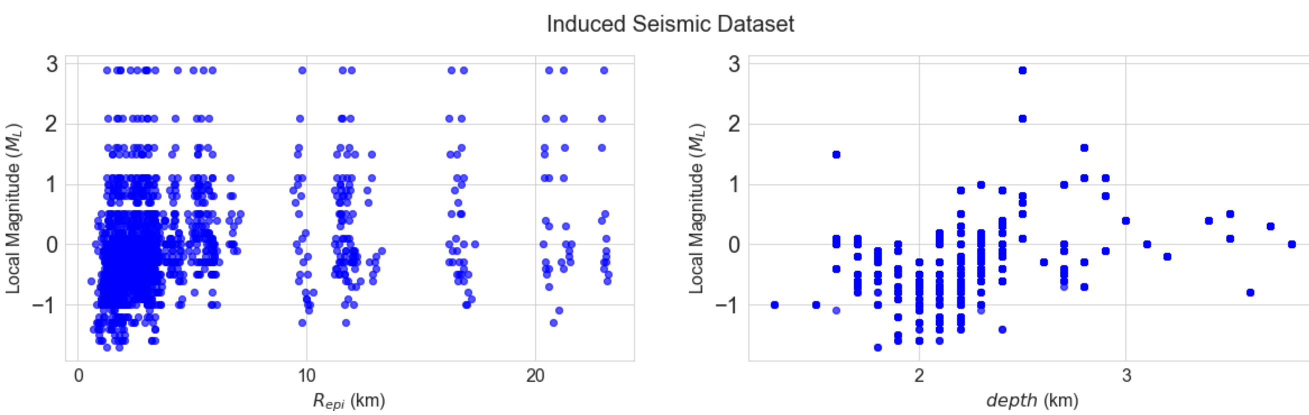

Figure 3. Earthquakes magnitude as function of distance (left) and depth (right) for induced dataset.

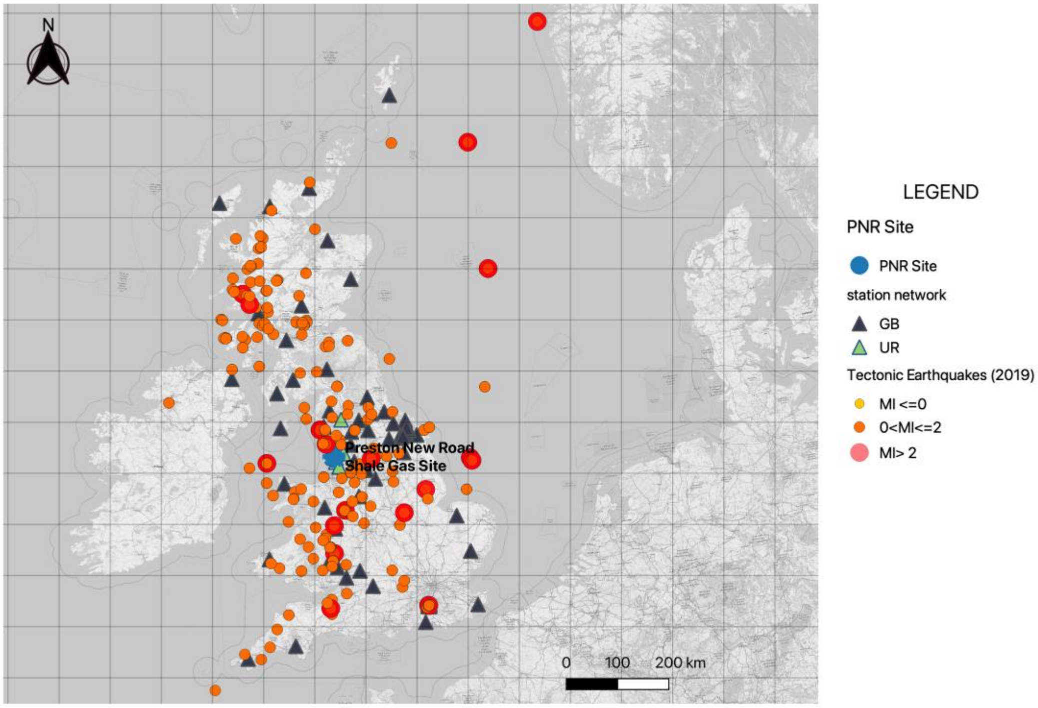

Figure 4. Map of stations and tectonic event locations (recorded in 2019) with local magnitude range -1.4 ≤ M_L < 4.6 (source: BGS website, last accessed: June 2022).

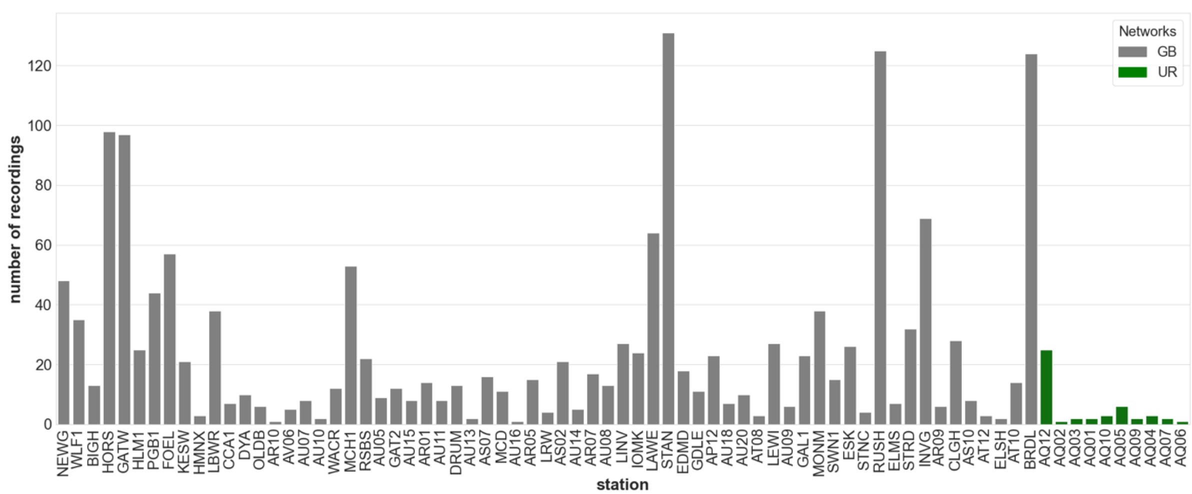

Figure 5. Number of recordings for each different stations for tectonic dataset. Colours indicate each different network.

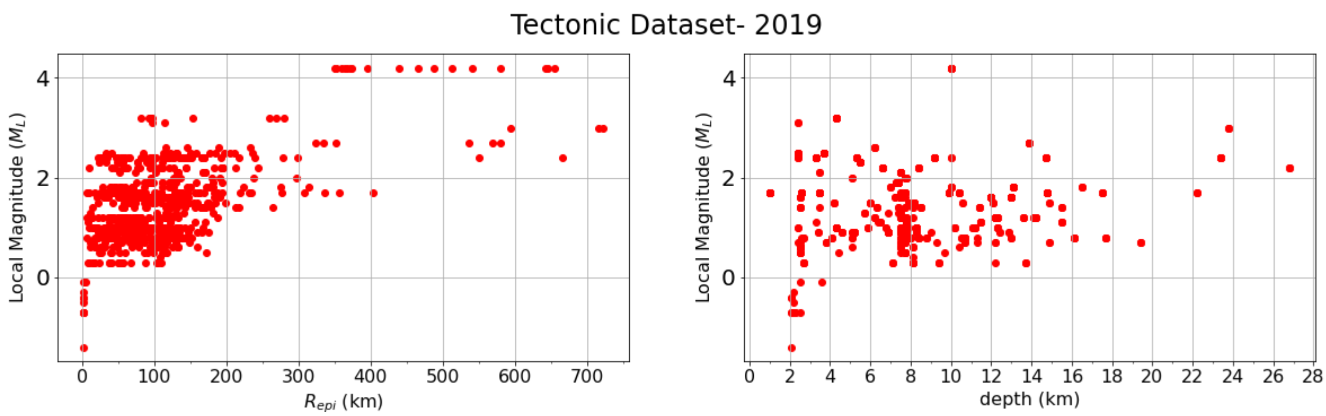

Figure 6. Earthquakes magnitude as function of distance (left) and depth (right) for tectonic dataset.

The original seismic records need to be pre-processed in order to calculate the observed peak ground acceleration (PGA) or peak ground velocity (PGV). Several steps are performed, including: (1) signal detrending, (2) removing the seismic instrument response, (3) recalculating the end of the signal, which corresponds with 95% of the cumulative energy; and (4) finding the highest amplitude value. The maximum absolute value of the amplitude on respective traces is used to calculate record-specific PGA and PGV.

Ground Motion Prediction Equation for Induced Seismicity, Case Study at Preston New Road, UK

Existing GMPE for Induced Seismicity at Preston New Road, UK

The performance analysis of the available ground motion models has been assessed at the PNR site by Edwards et al. (2021). The recorded ground motion has been compared with the prediction estimated using Atkinson (2015) and Douglas et al. (2013) models. The comparison of these involved residual analysis of both models, aiming to select most suitable model for subsequent adjustment using the referenced empirical approach (Bommer, et al., 2006; Atkinson, 2008). The first model tested was the GMPE of Douglas et al. (2013), developed specifically for geothermal induced seismicity, with data consisting of events with magnitude $\mathbf{M} \geq 1$ and R $< 30\ km$. According to Edwards et al. (2021), the ground motion overall is overpredicted. The overprediction tended to increase with the decrease of magnitude. These bias presumably due to significant regional differences. It is important to consider the site- specific or non-linearity effect, which is not addressed in the model proposed by Douglas et al. (2013). The significant misfit to local data and limited flexibility of the model for calibration to that data (for example, including only linear magnitude scaling) meant that this model is not selected for application in PNR site.

The next model tested was the Atkinson (2015) GMPE model (A15), developed based on the NGA-West2 dataset which consists of **M** 3 - 6 earthquakes. The majority of smaller earthquake are corresponding with Californian tectonic earthquakes which are not necessarily shallow. These records were limited up to 40 km hypocentral distance to focus on the near-source motion, typical of focus for induced seismicity. The A15 model is made for a rock reference site with Vs30 = 760 m/s. To adjust to local conditions at PNR, which has significantly lower Vs30, the site response model of Boore et al. (2014) was used (Vs_{30} ~200 - 300 m/s). The A15 GMPE model can be written as:

$$X = \Delta c_0 + \Delta c_1 \boldsymbol{M} + \Delta c_2 \boldsymbol{M}^2 + \Delta c_3 \log_{10} R + B_e + W_S \qquad (1)$$

with X is the ($\log_{10}$) peak acceleration for a given spectral ordinate, c_i are the coefficients, **M** is the moment magnitude and R is an effective distance, as defined in Atkinson (2015):

$$R = \sqrt{{R_{hyp}}^2 + \max(1, 10^{-0.28+0.19\,\boldsymbol{M}})^2} \qquad (2)$$

B_e in the equation 1 are the random effects for the events, and W_S are the station-specific random effects.

Based on the residual analysis by Edwards et al. (2021), a good fit is found at distances $R_{epi} > 5\ km$, but the model significantly underestimates at shorter distances. To minimise the sigma of prediction, calibration of the A15 model was therefore undertaken. This effort is in line with Bommer et al. (2006) and Atkinson (2008), which shows the improvements in the prediction of local ground motion estimates by using the referenced empirical approach. Edwards et al. (2021) perform the calibration using a mixed-effects regression. The adjustment, constrained by the data at available magnitude and distances, can be expressed as:

$$
\begin{aligned}
\log_{10} Y_{E20} &= d_0 + d_1\boldsymbol{M} + d_2\boldsymbol{M}^2 + d_3 \log_{10} R && \text{for } \boldsymbol{M} < 3 \\
\log_{10} Y_{E20} &= p_0 + p_1\boldsymbol{M} + p_2\boldsymbol{M}^2 + p_3 \log_{10} R && \text{for } 3 \leq \boldsymbol{M} < 4.5 \\
\log_{10} Y_{E20} &= Y_{A15} = c_0 + c_1\boldsymbol{M} + c_2\boldsymbol{M}^2 + \Delta c_3 \log_{10} R && \text{for } \mathbf{M} \geq 4.5
\end{aligned}
\tag{3}
$$

where d_i are the calibrated coefficients (Edwards et al., 2021), and p_i are linearly interpolated between original A15 coefficient (c_i) and calibrated coefficient (d_i), which can be written as:

$$
p_i = c_i + \frac{\boldsymbol{M} - 4.5}{3 - 4.5} \Delta c_i \tag{4}
$$

The difference is higher near-field short period motions in the calibrated A15 model, presented by Edwards et al. (2021), compared to original Atkinson (2015) model. The application of both models will be presented in the last chapter of this report (general discussion and conclusion).

Stochastic Ground Motion Model for Preston New Road, UK

Adapting and adjusting existing GMPEs may lead to predictions that are not robust and or potentially biased. One of the limitations of GMPE adjustment using the hybrid empirical method is that they must be converted into equivalent Fourier models by calculating minimum misfit Fourier Acceleration Spectrum (FAS) based models (Campbell, 2003; Scherbaum et al., 2006) or response spectra consistent FAS (Atik et al., 2014). Any physically based adjustment is inherently complex due to the simplified basis of empirical response spectra-based models. An alternative approach is by directly use FAS model based and shaking-duration, which related through stochastic simulation (Boore, 2003; Motazedian & Atkinson, 2005) or random-vibration theory (RVT) (Atkinson & Boore, 2006; Edwards & Fäh, 2013; Drouet & Cotton, 2015). Such models are calibrated based on physical properties of source, attenuation, and site conditions which are modelled or measured from earthquake recordings (e.g., Edwards et al., 2008; Drouet et al., 2011; Bommer, et al., 2016). The advantage of FAS based models (e.g., stochastic simulation model) are easier to adjust than the empirical GMPEs (Bora et al., 2013) and can easily linked to physical processes (Baltay et al., 2017). Besides, the epistemic uncertainty may also be easier to quantify: the physically interpretable parametric variations such as stress drop, attenuation, and site amplification can be specified as distributions rather than unique values. Taking the advantage of such stochastic simulation approaches, this study focuses on the development of physical-based ground motion model for induced seismicity.

The stochastic method proposed by Boore (2003) is a simple and powerful tool (so called Stochastic- Method SIMulation or SMSIM) to simulate ground motion by combining parametric or functional form of the ground motion's amplitude spectrum with a random phase spectrum. The stochastic method of Boore (2003) is used to simulate ground motion for the Preston New Road (PNR) site in terms of PGV and PGA. This method is relying on the knowledge of the expected Fourier spectrum of an earthquake recording with a given magnitude and distance. The spectrum of earthquake ground motion i recorded at station j that has been corrected with instrument response can be described as:

$$\Omega_{ij}(f) = E_i(f) \times P_{ij}(f) \times S_j(f) \tag{5}$$

where f is the frequency, and $E_i(f)$ is the amplitude spectrum of "Brune" source model, $P_{ij}(f)$ is the attenuation along the ray path, and $S_j(f)$ is the site term. By separating the spectrum into source, path, and site components, the models can be easily modified to account for specific situations.

The shape and the amplitude of the source spectrum should be specified as a function of earthquake size. The source model can be written as:

$$E_i(f) = \frac{\Omega_0}{1 + (f/f_c)^2} \tag{6}$$

The Ω_0 term contains seismic moment and other frequency–independent effects. The seismic moment (M_0) of a seismic record expressed as:

$$M_0 = \frac{4\,\pi\rho v^3 R_{hyp}\Omega_0}{F_s\, R_{\theta\phi}} \tag{7}$$

where ρ is the rock density at the source (2800 kg/m^3), v is the velocity in the source ($v =$ 2000 m/s), R_{hyp} is the hypocentral distance, and Ω_0 is the low- frequency plateu. F_s is the free surface amplification factor ($F_s = 2$ for normally incident SH waves and a good approximation for SV) and $R_{\theta\phi}$ is the average radiation pattern coefficient for S-waves (0.55) (Boore & Boatwright, 1984).

In the stochastic simulation approach, we used moment magnitude rather than seismic moment as a more familiar measure of earthquake size. The relation between seismic moment and moment magnitude is:

$$M_W = \frac{2}{3}\log M_0 - 6.03 \tag{8}$$

Since the earthquake sizes in the data catalogue were defined in terms of local magnitude (M_L), this value was converted to moment magnitude (M_W) by following the $M_L - M_W$ relationship explained in Edwards et al. (2021). For the smallest events:

$$M_W = \frac{2}{3}M_L + 0.833 \qquad (M_L < 1.5) \tag{9}$$

and for larger events, the $M_L - M_W$ relationship model from Grünthal et al. (2009)

$$M_W = 0.0376\, {M_L}^2 + 0.646\, M_L + 0.53 \qquad (M_L \geq 2.5) \tag{10}$$

with linear interpolation between both equation 9 and 10.

The path effect is representing the effect of geometrical spreading attenuation, and duration. The latest version (August 2021) of SMSIM allows the power of frequency in the Q model, therefore the attenuation along the ray path $[P_{ij}(f)]$ can be written as:

$$P_{ij}(f) = e^{-(\pi f^{1-\alpha} t^{*})} \tag{11}$$

where t^{*} is the attenuation parameter ($t^{*} = T/Q_0$, with T the travel time and Q_0 as the path-average quality factor at the reference frequency, here 1 Hz). α describes the frequency dependence of Q, with $Q(f) = Q_0 f^{\alpha}$.

The site effect $S_{ij}(f)$ is usually controlled by the amplification function $[A(f)]$ and diminution or damping function $[D(f)]$. This generally represented by a high frequency decay function or kappa, an exponential function to explain the additional high frequency attenuation as a characteristic of local site attenuation (Anderson & Hough, 1984).

Model Parameters

The ground motion can be simulated in two different ways: time-domain simulation and estimation using random vibration theory. In the time domain simulation, a time series envelope of Gaussian noise (with defined duration) is convolved with the target spectrum in the frequency domain. Returning to the time domain provides the simulated accelerogram. In practice, due to the random nature of the simulated time series, and the fact that we only need the peak amplitudes, random vibration theory is implemented to achieve the same result faster in this study. To perform the stochastic simulation, several parameters are defined. The attenuation model and kappa utilised in this study were defined from inversion scheme in the spectral fitting method detailed in Edwards et al. (2008) and (Suroyo & Edwards, 2023).

The spectral inversion scheme was performed for each individual record, following the steps presented in Figure 7, to fit t^{*}, f_c, Ω_0, and α (with a grid-search in the range 0-1), which allows us to calculate both frequency dependent and frequency independent Q measurements. This fitting approach was performed under the assumption that a single event from different recordings will share same seismic moment and Brune stress drop and are therefore fitted to an event-specific corner frequency (f_c). In Suroyo & Edwards (2023), the inversion scheme followed two steps:

(1) The first step of the inversion aimed to find the optimum value for α (frequency dependence of Q_0) by calculating the minimum chi-squared (${X_i}^2$) misfit (later denoted as α_{min}) and to calculate the frequency-independent Q_0 and κ_0. α_{min} was estimated by calculating the chi-squared (${X_i}^2$) misfit over the log spectral amplitudes for α within the range 0.0 - 1.0. The model misfit over the ensemble of observations for each given α can be quantified. In this step, a frequency-independent model (Q_0 and κ_0) was also determined using linear regression of t^* versus R_{hyp} for a given α = 0.

(2) The second inversion step was performed by fixing various elements based on the previous inversion results. A correction for frequency-independent κ_0 is applied and the final inversion performed using a grid search over f_c between 0 – 50 Hz, fixing discrete selections of α_{min} (lower limit of α_{min} : upper limit of α_{min}). The product of the second inversion is then the final $Q(f)$ and frequency-dependent $\kappa_{0,\zeta}$ model (i.e., Q_0, α, κ_0, and $\kappa_{0,\zeta}$).

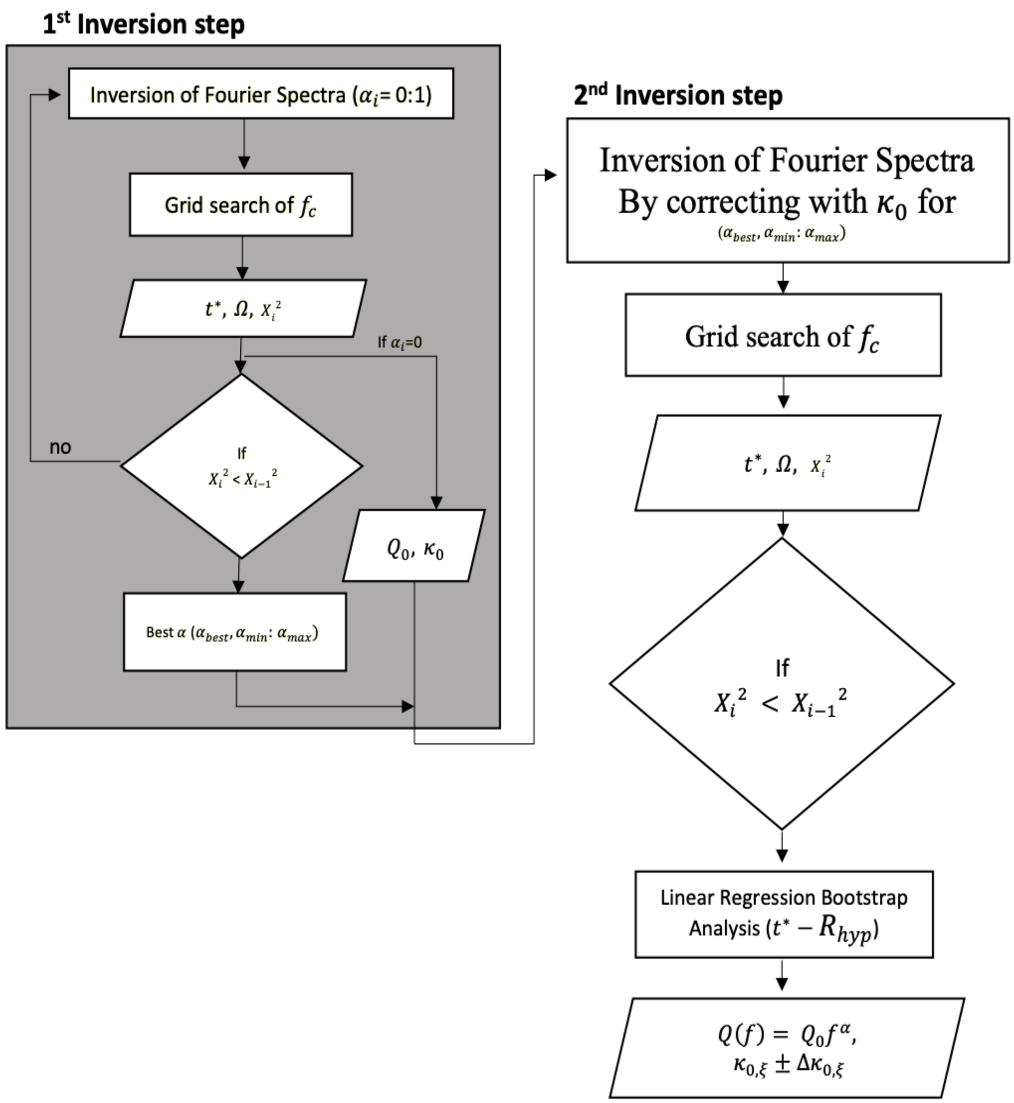

Figure 7. Flowchart of inversion process for the spectral fitting method.

The local $Q(f)$ obtained from the induced seismic sequences at Preston New Road (PNR) shale gas site, attributed to shallower layers in the crust, leads to a rapid rate of near-field decay (sudden loss in amplitude of earthquake signal over a short distances), with significantly stronger attenuation than observed for regional events. We furthermore find that estimates of seismic attenuation quality factor (Q_0) are non-unique to a given record, differing both with the method and the analysis windows used, particularly at high frequency (Figure 8). The lower overall $Q(f)$ (stronger attenuation) in the induced seismicity records and the decreasing efficiency of scattering effects at short-scale distances, justifies that directly adapting tectonic GMPE for induced seismicity will produce bias. Therefore, to predict ground motion models for shallow earthquakes, it is important to consider the rapid rate of attenuation observed at very near-distances. Besides the attenuation model, the site-specific high-frequency decay (κ_0) were obtained as a side product of the spectral fitting approach (Table 1). For stochastic simulation, we utilised the frequency-dependent Q model (result from stage 2 inversion scheme) and the classic or frequency-independent κ_0 (from stage 1 of inversion scheme).

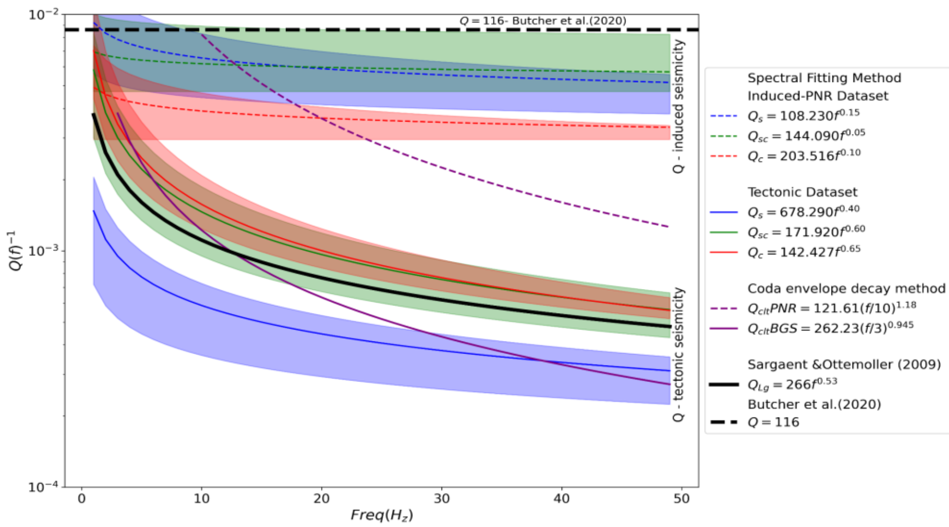

Figure 8. Attenuation model from spectral fitting and coda envelope decay method for induced and tectonic dataset. The shaded colour shows the confidence interval of the Q model (Suroyo & Edwards, 2023).

Table 1. Q_0 (1 Hz), α , $\kappa_{0,\zeta}(1Hz)$ and κ_0 from spectral fitting method for both induced and tectonic dataset (results for frequency-dependent and frequency-independent models from S wave windows).

	Frequency-dependent model **Final Model After Corrected with κ_0 (second inversion)**				**Frequency-independent model (initial inversion; $\alpha =$ 0)**	
	$\alpha \pm \Delta\alpha$	Q_0-Interval	$Q(f) = Q_0 f^{\alpha}$	$\kappa_{0,\zeta} \pm \Delta\kappa_{0,\zeta}$(s)	Q_0	$\kappa_0 \pm \Delta\kappa_0$(s)
Induced	0.15 ± 0.1	[67.8- 178.6]	$108.2\ f^{\ 0.15}$	0.033 ± 0.0013	169.6	0.018 ± 0.001

Tectonic	0.4 ± 0.1	[487.8- 1387.9]	$678.3\, f^{\,0.4}$	0.06 ± 0.012	2953.9	0.029 ± 0.003

In addition to the attenuation model, stress drop was estimated using:

$$\Delta\sigma = {}^{7}\!/_{16}\left(\frac{M_0}{(0.372 * {}^{V_s}\!/_{f_c})^3}\right) \tag{12}$$

Stress drop describes the difference in shear stress on a fault before and after an earthquake, which can have a strong influence on ground motions for frequencies of engineering concern (Hanks, 1979; and Boore, 1983). Whil se Huang et al. (2017) suggests that ground motion prediction equations developed for tectonic earthquakes can be applied to induced earthquakes (after properly considering the effects of depth and faulting style), in some cases, stress drop of induced earthquakes is not comparable with the stress drop from tectonic earthquakes. Hough (2014) infers that induced earthquakes have lower stress drops than tectonic earthquakes based on a comparison of non-instrumental “Did You Feel It?” intensities. In this study, we take the power 10 of log average stress drop from each different dataset (tectonic and induced seismicity) (Figure 9). The stochastic simulation is then performed using stress drop equal to 7.0 Bar for tectonic seismic and 2 Bar for induced seismicity, with other parameters detailed in Table 2.

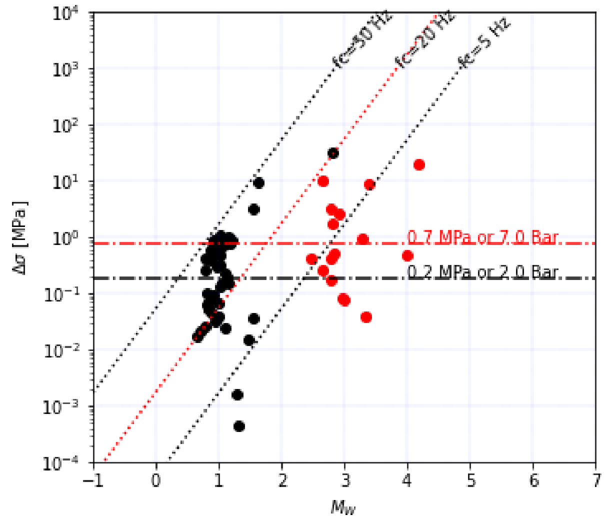

Figure 9. Stress drops vs moment magnitude for induced dataset (black) and tectonic dataset (red) from spectral fitting approach.

Table 2. Summary of input parameters for SMSIM in this study.

Parameter	Model	Description
Rho (gm/cc)	2.8	Density of the medium
Beta (km/s)	2.7 for induced dataset and 3.5 for tectonic dataset	Velocity of the medium
Partition factor (prtitn)	0.71	Partition factor
Radiation pattern	0.55	Radiation pattern
fs	2.0	Free surface factor
Stress specification	stress = stressc*10.0**(dlsdm*(amag-amagc)), where stressc = 100.0, dlsdm = 0.0, amagc = 7.0, fbdfa=4.0	Parameters control the scaling of spectral amplitudes with source size. Stresssc: stress dlsdm: derivative of log sigma with respect to magnitude amagc: critical magnitude fbdfa: corner frequency fb divided by fa
Geometrical spreading	r_ref =1.0 km, nsegs = 3 rlow (1) = 1.0, a_s = -1.0, b_s= 0.0, m_s (1) =6.5 rlow (2) = 70.0, a_s = 0.0, b_s= 0.0, m_s (2) =6.5	Parameters control the geometrical spreading. R_ref: reference distance Nsegs: number of segments, each segment starting at rlow. a_s, b_s, and m_s are the coefficients of the slope of linen segment, can be written as: $slope\ (j) = a\_s\ (j) + b\_s(j)(M - m\_s(j))$

	rlow (3) = 130.0, a_s = -0.5, b_s= 0.0, m_s (3) =6.5	
Anelastic attenuation model (Q)	fr1=0.1, Qr1=108.2 (for induced), 678.3 (for tectonic) sl=0.15(for induced), 0.4 (for tectonic) ft1=1.0, ft2=1.0, fr2=1.0, qr2= 108.2 (for induced), 678.3 (for tectonic) s2=0.15(for induced), 0.4 (for tectonic) c_q =2.7(for induced), 3.5 (for tectonic)	$Q(f)$is given by a piecewise continuous set of three straight lines in log Q and log f space. The first and third lines have slopes of s1and s2 and values of Qr1 and Qr2 at reference frequencies fr1 and fr2, respectively. ft1, ft2 are the transition frequencies. c_q is the velocity used in deriving the Q function.
Source duration	0.5 (weights of 1/fa, 1/fb)	Source duration
Path duration	nknots = 4 rdur (1) = 0.0, dur (1) = 0.0 rdur (2) = 10.0, dur (2) = 0.0 rdur (3) = 70.0, dur (3) = 9.6 rdur (4) = 130.0, dur (4) = 7.8 slope of last segment =0.04	specification of the path duration nknots is the number of intersections between line segments.
Crustal amplification	Namps= 5 famp (1) = 0.1, amp (1) = 1.0 famp (2) = 1.0, amp (2) = 1.5 famp (3) = 2.0, amp (3) = 2.0 famp (4) = 5.0, amp (4) = 2.5 famp (5) = 10, amp (5) = 3.0	Site amplification is approximated by a series of straight-line segments in log amplification, log frequency space, connecting the values famp, amp. Namps is the number of segments.
Site diminution parameters	fmax=50.0, kappa= 0.018(for induced), 0.029 (for tectonic)	Site diminution factor

General Discussion and Conclusions

Better determination of seismic hazard is one of the important factors for a better risk assessment. Seismic hazard assessment by adapting and adjusting the existing GMPE for near field- shallow earthquakes has been evaluated in this study specifically for PNR site. In this work, the attenuation parameter known as the quality factor (Q) and site-specific high-frequency decay (κ_0) of UK tectonic and PNR induced seismicity datasets from previous study by Suroyo & Edwards (2023) were incorporated to develop a new physical-based ground motion model.

The Fourier spectrum of the ground motion is essential information for developing a physical-based ground motion model, which reflect the contributions of the earthquake source, wave propagation, and site amplification. A preliminary study to better understand source, path, and site characteristics for induced seismicity at the PNR site and UK tectonic seismicity has been conducted by Suroyo & Edwards (2023) using spectral fitting approach. For the path term, attenuation models obtained are $Q_T = 678.3f^{0.4}$ and $Q_I = 108.2f^{0.15}$for tectonic and induced seismicity, respectively. Average site-specific high-frequency decay (κ_0) noted as 0.029 s for tectonic and 0.018 s for induced dataset (Suroyo & Edwards, 2023). These model parameters are then used to perform the stochastic simulation. This report presented the comparison between simulated PGA and PGV with empirical prediction following GMPEs from Atkinson (2015), and a calibrated version of Atkinson's GMPE (in this study known as the Edwards et al. (2021) model).

The difference between the predicted value and the observation (residual value) is presented in Figures 10 and 12. Figures 11 and 13 show additional illustrations of the binned average and its standard deviation to represent the mean residual value for a given bin and the variability within the bin. The results indicate that the existing GMPE for induced seismicity developed by Atkinson (2015) underpredicts the ground motion at the PNR site, while the calibrated GMPE model by Edwards et al. (2021) shows improved prediction, despite the uncertainty that follows the prediction. This emphasizes the importance of local calibration or local-specific in predicting ground motion. Residuals of the simulated PGA and PGV for induced dataset show a relatively good fit at lower magnitudes and slightly underestimate the observation at magnitudes > 1.5 (Figures 10 and 11). This might explain the necessity of using the scaling of stress drop with magnitude in the simulation.

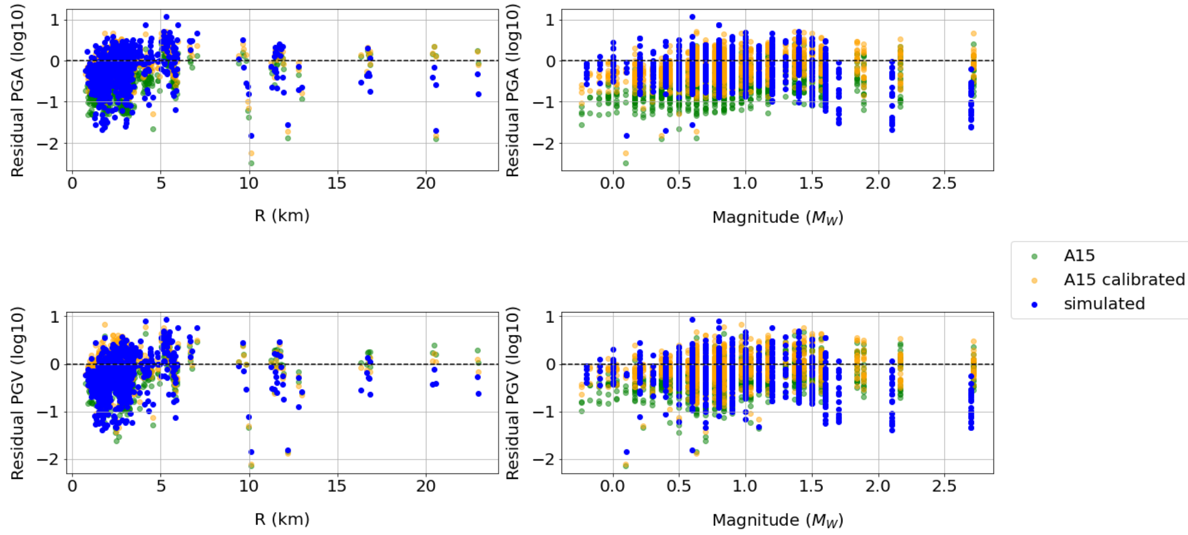

Figure 10.Residuals [in log-10] for PGV (below) and PGA (upper) versus magnitude (right) and distance (left) obtained from PNR- induced dataset (2018-2019). Green dots refer to the calculated PGV and PGA using Atkinson (2015) model, while yellow dots correspond to calibrated model (Edwards et al., 2021) and blue dots are the simulated PGV and PGA.

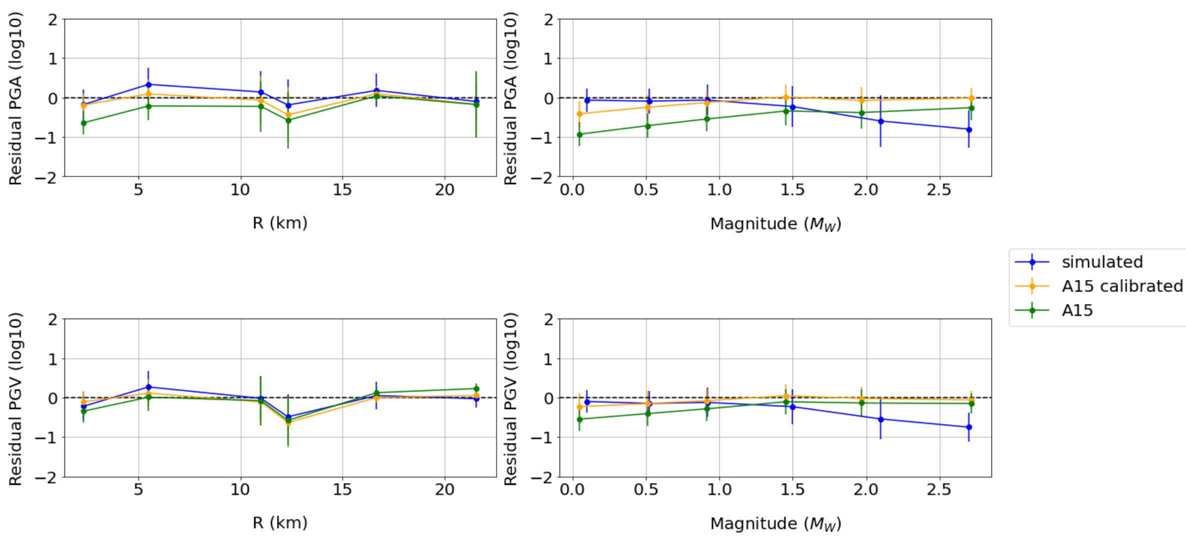

Figure 11.Binned average of residual values [in log-10] for PGV (below) and PGA (upper) versus magnitude (right) and distance (left) obtained from PNR- induced dataset (2018-2019). Green dots refer to the calculated PGV and PGA using Atkinson (2015) model, while yellow dots correspond to calibrated model (Edwards et al., 2021) and blue dots are the simulated PGV and PGA. Number of bins =6, with interval width equal to 3.77 km for residual vs distance (left) and 0.5 M_W for residual vs magnitude (right).

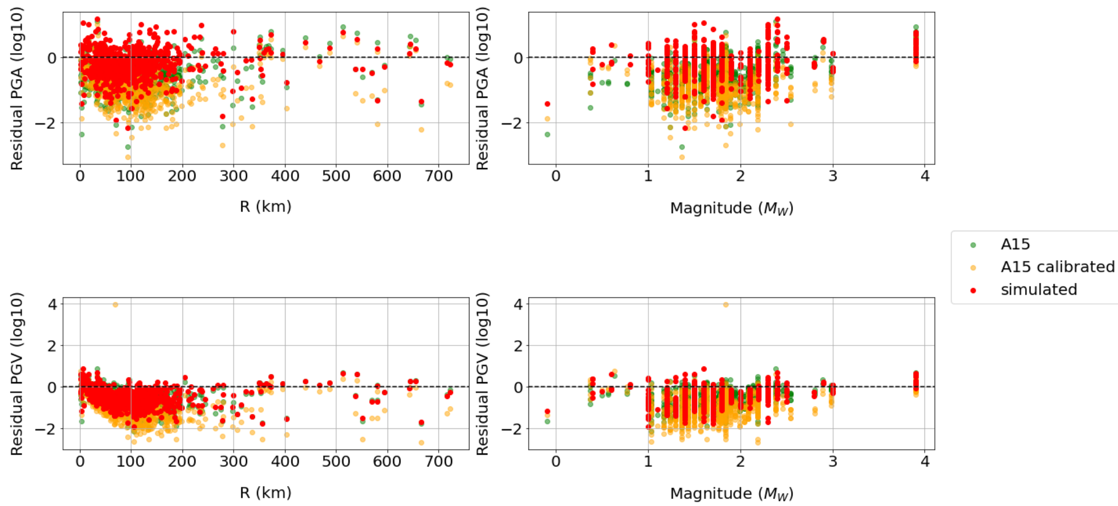

Figure 12. Residuals [in log-10] for PGV (below) and PGA (upper) versus magnitude (right) and distance (left) obtained from UK tectonic dataset (2019). Green dots refer to the calculated PGV and PGA using Atkinson (2015) model, while yellow dots correspond to calibrated (Edwards et al., 2021) and red dots are the simulated PGV and PGA.

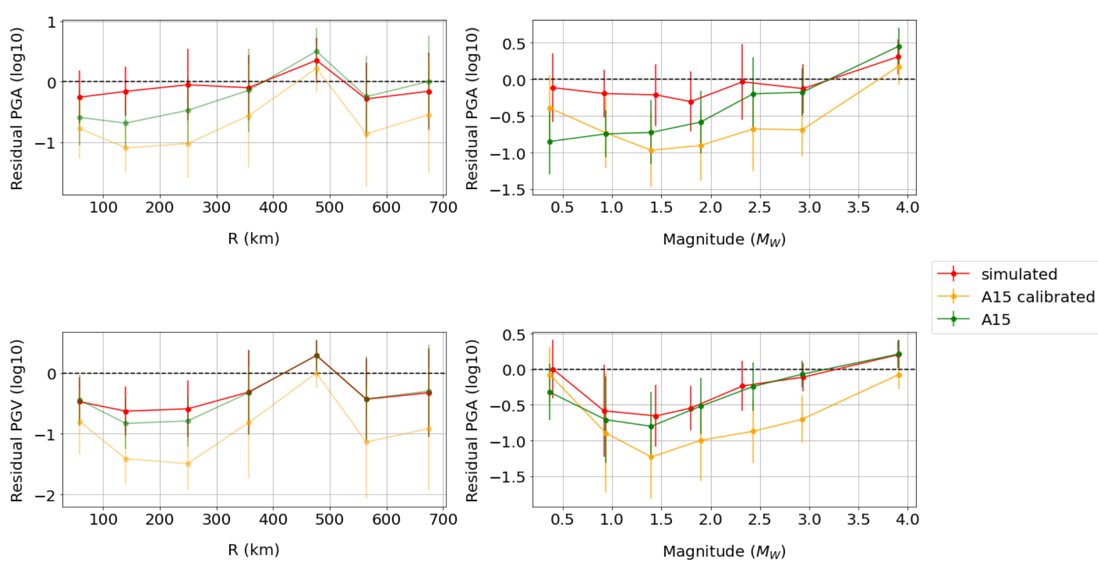

Figure 13.Binned average of residual values [in log-10] for PGV (below) and PGA (upper) versus magnitude (right) and distance (left) obtained from UK tectonic dataset (2019). Green dots refer to the calculated PGV and PGA using Atkinson (2015) model, while yellow dots correspond to calibrated (Edwards et al., 2021) and red dots are the simulated PGV and PGA. Number of bins =7, with interval width equal to 102.87 km for residual vs distance (left) and 0.6 M_W for residual vs magnitude (right).

Higher variability is observed in the residual results for tectonic dataset (Figures 12 &13). It is noted that the empirical prediction produces slightly lower residual value compared with simulated prediction. Overall, the residual plot of the tectonic dataset shows underprediction for both empirical (Atkinson's model and calibrated model) and simulated prediction. Examples of PSA with respect to period for two different tectonic events: 2.9 M_W recorded at 183.72 km and 1.5 M_w at 102.4 km distances with two different stress drop inputs are given in Figure 14.

The comparison of model of Atkinson (2015), calibrated model by Edwards et al. (2021), simulated PGV, and observed PGV for two events (2.9 and 1.5 M_W) is illustrated in the Figure 15, in addition to a similar comparison of two examples of induced seismic events (0.4 and 1.6 M_w). The comparison for induced seismicity case (Figure 15a) reveals that the empirical GMPEs (A15, and calibrated) are slightly overestimate the observation at $R > 5$ km for 1.5 M_W event, while the simulated PGV appears to give promising results. However, the simulated PGV shows that the rapid decay of near-field motions is confined to the majority of small ($M_L < 1.5$) events which is shown by the underprediction at a near distance ($R< 5$ km) for 1.6 M_W earthquake, although the simulated PGV is comparable to the observed PGV for smaller events. As for the tectonic earthquake case shown in Figure 15.b, the empirical and stochastic prediction tend to underpredict, particularly at distance greater than 40 km. The underprediction founds to be higher at a lower magnitude. This can be due to the selection of the GMPE model, which is better suited for the induced seismic case. The GMPE models used in this study were developed and calibrated for near-source distance earthquakes ($R< 40$ km), with near-source distance saturation considered. In fact, for tectonic earthquakes, as the distance increases, the near-source distance saturation should be disregarded. Although the simulated PGV predicts better than the empirical PGV, the bias of the prediction is still large, and the simulation needs to be optimised.

Finally, this work demonstrates the different characteristics of ground motion model for near field- shallow earthquake and the deeper tectonic earthquake. Selecting proper and suitable ground motion model is a crucial part for hazard assessment. Our result illustrates the use of near-source distance saturation for large magnitude (tectonic) events may result in bias, and directly adapting tectonic GMPEs for induced seismicity is also tricky and not a suitable solution. We suggest implementing the rapid decay of near-field motions to lower magnitude ($ML < 1.5$) and short distance events. Further analysis about the uncertainty and variability of the input model parameter to minimise the misfit and better predict the ground motion is needed.

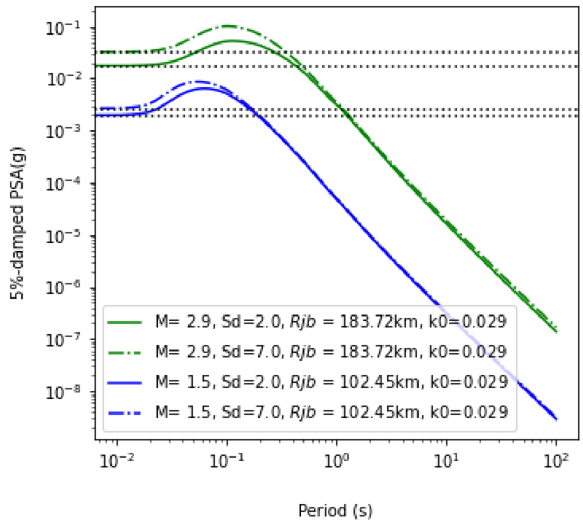

Figure 14.Response spectra computed with time-domain simulations for 2.9 and 1.5 M_w (tectonic events). Black dashed lines show the corresponding PGA values.

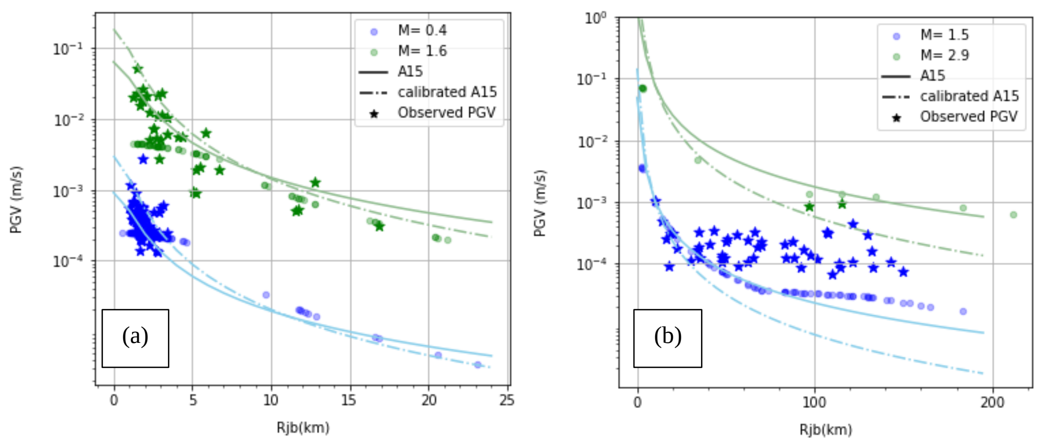

Figure 15. Observed PGV for: (a) induced dataset with magnitude 0.4 M_W and 1.6 M_W and (b) tectonic dataset with magnitude 1.5 M_W and 2.9 M_W, compared to the model of Atkinson (2015), calibrated model by Edwards et al. (2021), and simulated PGV. Circles are simulated values.

References

Anderson, J., & Hough, S. (1984). A model for the shape of the Fourier amplitudespectrum of acceleration at high frequencies. *Bulletin of the Seismological Society of America, 74*(5), 1969-1993.

Atik, L. A., Kottke, A., Abrahamson, N., & Hollenback, J. (2014). Kappa (κ) Scaling of Ground-Motion Prediction Equations Using an Inverse Random

Vibration Theory Approach. *Bulletin of the Seismological Society of AmericaSearch Dropdown Menu, 104*(1), 336-346.

Atkinson, G. (2008). Ground-motion prediction equations for eastern North America from a referenced empirical approach: Implications for epistemic uncertainty. *Bulletin of Seismological Society of America, 98*(3), 1304-1318.

Atkinson, G. M. (2015). Ground-motion prediction equation for small-to-moderate events at short hypocentral distances, with application to induced-seismicity hazards. *Bulletion of the Seisological Society of America, 105*(2A), 981-992.

Atkinson, G. M., & and Assatourians, K. (2017). Are ground-motion models derived from natural events applicable to the estimation of expected motions for induced earthquakes? *Seismological Research Letters, 88*(2A), 430-441.

Atkinson, G. M., & Assatourians, K. (2017). Are ground-motion models derived from natural events applicable to the estimation of expected motions for induced earthquakes? *Seismological Research lETTERS, 88*(2A), 430-441.

Atkinson, G. M., & Boore, D. M. (2006). Earthquake Ground-Motion Prediction Equations for Eastern North America. *Bulletin of the Seismological Society of America, 966*(6), 2181-2205.

Baltay, A., & Hanks, T. (2014). Understanding the magnitude dependence of PGA and PGV in NGA-West 2 data. *Bulletin of the Seismologcal Society of America*, 2851-2865.

Baltay, A., Hanks, T., & Abrahamson, N. (2017). Uncertainty, variability, and earthquake physics in Ground-Motion prediction Equations. *Bull. seism. Soc. Am*.

Bent, A. L., S. Halchuk, V. Peci, K. E. Butler, K. B. Burke, J. Adams, N. Dahal, and S. Hayek (2017). The McAdam, New Brunswick, Earthquake Swarms of 2012 and 2015– 2016: Extremely Shallow, Natural Events, Seismol Res Lett 88, no. 6, 1586 1600, doi: 10.1785/0220170071.

Bommer, J. J. (2022). Earthquake hazard and risk analysis for natural and induced seismicity: towaards objective assessments in the face of uncertainty. *Bulletin of Earthquake Engineering, 20*, 2825-3069.

Bommer, J. J., Dost, B., Edwards, B., Stafford, P. J., Elk, J. v., Doornhof, D., & Ntinalexis, a. M. (2016). Developing an Application-Specific Ground-Motion Model for Induced Seismicity. *Bulletin of the Seismological Society of America, 106*(1), 158-173.

Bommer, J. J., Oates, S., Cepeda, J., Lindholm, C., Bird, J., Torres, R., Marroquin, G., Rivas, J. (2006). Control of hazard due to seismicity induced by a hot fractured rock geothermal project. *Engineering Geology, 90*(3), 708-723.

Bommer, J. J., Stafford, P., Alarćon, J., & Akkar, S. (2007). The influence of magnitude range on empirical ground-motion prediction. *Bulletin of the Seismology Society of America*, 2152-2170.

Bora, S., Scherbaum, F., Kuehn, N., and Stafford, P. (2013). Fourier spectral- and duration models for the generation of response spectra adjustable to different source-, propagation-, and site conditions. *Bull. Earthq. Eng.*, 1-27.

Boore, D. (2003). Simulation of Ground Motion Using the Stochastic Method. *Pure appl. geophys, 160*, 653-676.

Boore, D. M. (1983). Stochastic Simulation of High-Frequency Ground Motions Based on Seismological Models of the Radiated Spectra. *Bulletin of the Seismological Society of America, 73*(6), 1865-1894.

Boore, D. M., & Boatwright, J. (1984). Average body-wave radiation coefficients. *Bull. Seism.Soc. Am*, *74*, 2035-2039.

Bormann, P., Baumbach, M., Bock, G., Grosser, H., Choy, G., & J., a. B. (2002). Chapter 3: Seismic Sources and Source Parameters. In P. (. Bormann, *IASPEI: New manual of Seismological Observatory Practice 1*. Potsdam, Germany: GeoForschungsZentrum Potsdam.

Campbell, K. (2003). Prediction of strong ground motion using the hybrid empirical method and its use in the development of ground-motion (attenuation) relations in eastern North America. *Bulletin of Seismological Society of America, 93*(3), 1012-1033.

Chiou, B., & Youngs, R. (2014). Update of the Chiou and Youngs NGA model for the average horizontal component of peak ground motion and response spectra. . *Earthquake Spectra*, 1117-1153.

Chiou, B., Youngs, R., Abrahamson, N., & Addo, K. (2010). Ground-motion attenuation for small-to-moderate shallow crustal earthquakes in California and its implications on regionalization of ground -motion prediction models. *Earthquake Spectra*, 907-926.

Davis, S., & Frolich, C. (1993). Did (or will) fluid injection cause earthquakes? Criteria for a rational assessment. *Seismology Research Letters*, 207-224.

Dost, B., Eck, T. van, & Haak, H. (2004). Scaling of peak ground acceleration and peak ground velocity recorded in The Netherlands. *Bolletino di Geofisicia Teorica ed Applicata*, *45*(3), 153-168.

Douglas, J., & Jousset, P. (2011). Modeling the difference in ground-motion magnitude-scaling in small and large earthquakes. *Seismological Research Letters*, 504-508.

Douglas, J., Edwards, B., Convertito, V., Sharma, N., Tramell, A., Kraaijpoel, D., Cabrera, N.M., Maercklin, N., and Troise, C. (2013). Predicting ground motion from induced earthquakes in geothermal areas. *Bull. Seismol. Soc. Am.*, *103*(3), 1875 - 1897.

Drouet, S., & Cotton, F. (2015). Regional Stochastic GMPEs in Low-Seismicity Areas: Scaling and Aleatory Variability Analysis—Application to the French Alps. *Bulletin of the Seismological Society of America*, *105*(4), 1883-1902.

Drouet, S., Bouin, M.-P., & Cotton, F. (2011). New moment magnitude scale, evidence of stress drop magnitude scaling and stochastic ground motion model for the French West Indies. *Geophysical Journal International*, *187*(3), 1625-1644.

Edwards, B., & Fäh, D. (2013). A Stochastic Ground-Motion Model for Switzerland. *Bulletin of Seismological Society of America*, *103*(1), 78-98.

Edwards, B., Crowley, H., Pinho, R., & Bommer, J. J. (2021). Seismic Hazard and Risk due to Induced Earthquakes at a Shale Gas Site. *Bulletin of the Seismological Society of America* .

Edwards, B., Rietbrock, A., Bommer, J. J., & Baptie, B. (2008). The Acquisition of Source, Path, and Site Effects from Microearthquake Recordings Using Q Tomography: Application to the United Kingdom. *Bulletin of the Seismological Society of America*, *98*, 1915-1935.

Farajpor, Z. (2021). A Ground-Motion Prediction Model for Small-to-Moderate Induced Earthquakes for Central and Eastern United States and Ground Motion Model Ranking. *Electronic Theses and Dissertations*.

Grünthal, G., Wahlström, R., & Stromeyer, D. (2009). The unified catalogue of earthquakes in central, northern, and northwestern Europe (CENEC)—updated and expanded to the last millennium. *106*(2), 653-664.

Grazier, V. (2017). Alternative (G-16v2) ground-motion prediction equations for Central and Eastern North America. *Bulletin of the Seismological Society of America*, *107*, 869-886.

Gupta, A., Baker, J. W., & and Ellsworth, W. L. (2017). Assessing ground-motion amplitudes and attenuation for small-to-moderate induced and tectonic earthquakes in the central and eastern United States. *Seismological Research Letters, 88*(5), 1379-1389.

Hanks, T. C. (1979). b-values and w-'Y seismic source models: Implications for tectonic stress variations along active crustal fault zones and the estimation of high-frequency strong ground motion. *J. Geophys. Res.*,

Hicks, S.P., Verdon, J., Baptie, B., Luckett, R., Mildon, Z.K. and Gernon, T., 2019. A shallow earthquake swarm close to hydrocarbon activities: Discriminating between natural and induced causes for the 2018–2019 Surrey, United Kingdom, earthquake sequence. *Seismological Research Letters*, *90*(6), pp.2095-2110

HiQuake. (2022, 07 11). *The Human-Induced Earthquake Database*. Retrieved 10 13, 2022, from https://inducedearthquakes.org/

Hough, S. E. (2014). Shaking from injection-induced earthquakes in the central and eastern United States. *Bull. Seismol. Soc. Am*, *104*(5), 2619–2626,.

Huang, Y., Ellsworth, W. L., & Beroza, G. C. (2017). Stress drops of induced and tectonic earthquakes in the central United States are indistinguishable. *Science Advances*, *3*(8).

McNamara, D. E., Petersen, M. D., Thompson, E. M., Powers, P. M., Shumway, A. M., Hoover, S. M., Moschetti, M. P., and Wolin, E. (2019). Evaluation of Ground-Motion Models for USGS Seismic Hazard Forecasts: Induced and Tectonic Earthquakes in the Central and Eastern United States Evaluation of GMMs for USGS Seismic Hazard Forecasts. *Bulletin of the Seismological Society of America*, *109*(1), 322-335.

Motazedian, D., & Atkinson, G. M. (2005). Stochastic Finite-Fault Modeling Based on a Dynamic Corner Frequency. *Bulletin of the Seismological Society of America,*, *95*(3), 995-1010.

Müller, B., M.-L. Doan, T. H. Goebel, Y. Liu, P. Martínez-Garzón, T. Mitchell, and I. Zaliapin (2021), Understanding and anticipating induced seismicity, *Eos, 102*, https://doi.org/10.1029/2021EO161325. Published on 30 July 2021.

McGarr, A., David Simpson, L. Seeber. (2002). Case Histories of Induced and Triggered Seismicity.*International Handbook of Earthquake and Engineering Seismology*,81A, 647-661.

Rietbrock, A., Strasser, F., & Edwards, B. (2013). A stochastic earthquake ground-motion predictioin model for tthe United Kingdom. *Bulletin of Seismological Society of America, 103*(1), 5-57.

Scerbaum, F., Cotton, F., & Staedke, H. (2006). The Estimation of Minimum-Misfit Stochastic Models from Empirical Ground-Motion Prediction Equations. *Bulletin of Seismological Society of America, 96*(2), 427-445.

Shapiro, S. D. (2010). Seismogenic indexand magnitude probability of earthquakes induced during reservoir fluid simulations. *Lead Edge*, 304-309.

Sharma, N., Convertito, V., Maercklin, N., & Zollo, A. (2014). Source-scaling relationships for the simulation of rupture geometry within probabilistic seismic-hazard analysis. *Bull. Seismol. Soc. Am., 104*(4), 1620 - 1634.

Suroyo, P., & Edwards, B. (2023). Rapid Near Field Attenuation of Ground Motion from Shallow Induced Earthquake, Case Study: Preston New Road, UK. *Sesimological Research Letters.*

Walters, R. J., Zobback, M. D., Baker, J. W., & Beroza, G. (2015). Characterizing and Responding to Seismic Risk Associated with Earthquakes Potentially Triggered by Fluid Disposal and Hydraulic Fracturing. *Seismological Research Letters*, 1110-1118.

Wilson, M., Foulger, G., Glluyas, J., & Julian, B. (2017). HiQuake: The Human-Induced Earthquake Database. *Seismological Research Letters*, 1560-1565.

Yenier, E., & and Atkinson, G. M. (2015). Regionally adjustable generic ground-motion prediction equation based on equivalent point-source simulations: Application to central and eastern North America. *Bulletin of the Seismological Society of America, 105*(4), 1989–2009.

List of Figures

List of Table